Phonocatalysis. An ab initio simulation experiment

Kwangnam Kim and Massoud Kaviany[a]
University of Michigan, Department of Mechanical Engineering, Ann Arbor, MI 48105-2125, USA

(Received 21 March 2016; accepted 19 June 2016; published online 27 June 2016)

Using simulations, we postulate and show that heterocatalysis on large-bandgap semiconductors can be controlled by substrate phonons, i.e., phonocatalysis. With *ab initio* calculations, including molecular dynamic simulations, the chemisorbed dissociation of XeF_6 on h-BN surface leads to formation of XeF_4 and two surface F/h-BN bonds. The reaction pathway and energies are evaluated, and the sorption and reaction emitted/absorbed phonons are identified through spectral analysis of the surface atomic motion. Due to large bandgap, the atomic vibration (phonon) energy transfer channels dominate and among them is the match between the F/h-BN covalent bond stretching and the optical phonons. We show that the chemisorbed dissociation (the pathway activation ascent) requires absorption of large-energy optical phonons. Then using progressively heavier isotopes of B and N atoms, we show that limiting these high-energy optical phonons inhibits the chemisorbed dissociation, i.e., controllable phonocatalysis. [http://dx.doi.org/10.1063/1.4955054]

I. INTRODUCTION

Role of phonons in metallic surface chemisorption, as an energy transfer channel, has been studied with the *ab initio* calculations[1] and with model Hamiltonians[2] showing that interaction with phonons is the main energy channel for the relaxation of the hot H adatoms generated by the dissociative chemisorption on Pd(100)[1]. The role of multiphonon emission in the energy channel was studied by reconstructing the Hamiltonian which includes the vibrational coupling between the adatom and the metal atoms and significantly decreases the strength of interaction, reducing the multiphonon emission rate.[2] There it was found that the dominate energy relaxation channel is the electron-hole excitation for Pt-CO vibrational mode. In photocatalysis, with increase in temperature the nonradiative recombination of photogenerated charge carriers dominates the energy transfer due to population increase of the high-energy phonons.[3] Phonon absorption/emission processes can dominate exchange of energy of atoms and molecules colliding with the surface, as shown with the surface scattering theory introducing the Fermi golden rule with phonons and rotational and internal mode excitations in the energy transfer channel.[4] The high-resolution electron energy loss spectroscopy of dissociative chemisorption of H on Ir(111), shows that the broad linewidth of low-frequency band is due to the vibrational coupling between substrate phonons and delocalized adatom motions.[5] The related analysis shows that the low-vibrational frequency mode of adsorbate is embedded in the continuous modes of the substrate phonon with broad resonance and short lifetime, and the high-frequency mode shows a sharp and localized mode with long lifetime due to the requirement of multiphonon interaction.[6]

While the roles of phonon in chemisorption have been investigated mostly as posteriori, here we pursue the control of chemisorbed dissociation by a controlled study of the substrate phonons. The main concept of phonocatalysis is the dissociative chemisorption reaction where the energy transfer channel to/from substrate is only by phonon, and this catalytic reaction can be managed

[a]Electronic mail: kaviany@umich.edu

by controlling phonon energies using heavier substrate isotopes to reduce the phonon cutoff frequency (maximum optical phonon energy). This change in substrate atomic mass does not change the electronic force field which controls the reaction. Surface-mediated energy conversions of molecules may involve interactions with photons, electron-hole pairs, and multiple phonons. The role of photon is ignored here since there is no photon source (as compared to photocatalysis), and since the role of radiative decays in the reaction can be neglected (compared to electrons and phonon interactions[7]). The effect of electron-hole pairs also can be omitted when insulators or large-bandgap semiconductors (this study) are considered as a substrate. Thus, phonon-energy channel is the most important mechanism for the sorption and reaction process of molecules. We explore the contribution of this phonon-energy channel on the dissociative chemisorption by controlling the substrate phonons, i.e., atomic dissociation from parent molecule controlled by phonons, using progressively heavier isotopes of B and N atoms. With *ab initio* calculations, the reaction pathway and energies are assessed and molecular dynamics simulations are implemented to demonstrate the controlled chemisorbed dissociation with spectral analysis of the surface atomic motion.

To show the controllable phonocatalysis, h-BN and XeF_6 are selected as a substrate and adsorbent, where the h-BN hexagonal lattice, layered structure allows for a smooth surface, weak van der Waals forces between layers and strong in-plane covalent bond (high phonon cutoff energy of 200 meV). h-BN is a semiconductor with large bandgap (we predict 4.0 eV, in good agreement with available results)[8–10] and has high chemical stability (up to 1300 K in air). Its lattice constants calculated are 2.49 Å in-plane and 6.46 Å across-plane consistent to reported results[11,12] (see Section II for the calculation methods), and obtained phonon density of states D_p is also in a good agreement with reported results.[11–14] We verify that the difference between the calculated bulk and thin film D_p are negligible (Fig. 1) due to dominance of in-plane vibrations, and will not affect to our results and discussions. Note that the thin film h-BN shows low and high-energy enhancement and scatter in D_p due to the substrate phonon.[15,16]

Xenon and Fluorine have eight and seven valence electrons, respectively, so XeF_6 consists of six Xe-F bonds and one lone electron pair as shown in Fig. 2(a). Three electrons in the $5p$ orbital

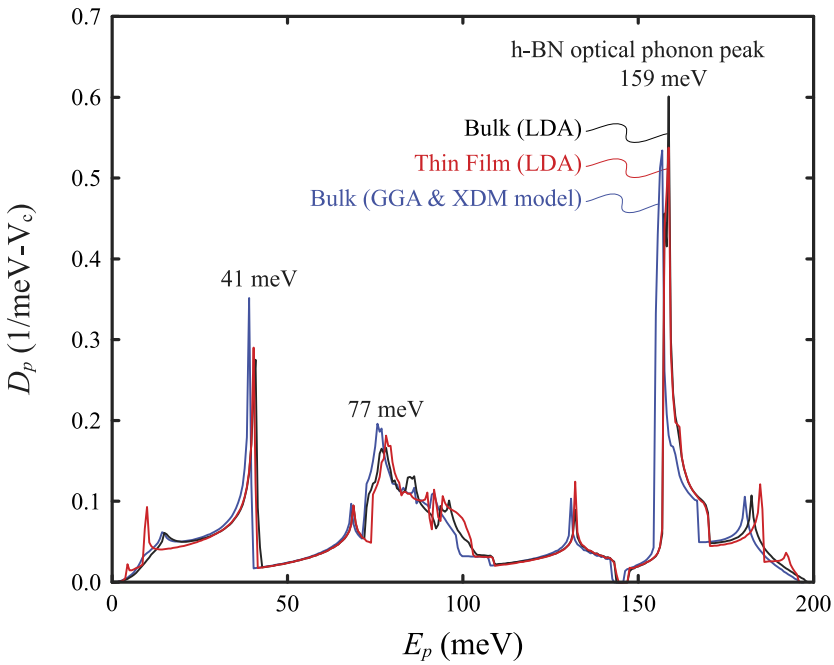

FIG. 1. Phonon density of states D_p for the bulk and thin film h-BN structures. The thin film shows some variations near 77 meV and enhancements near the lowest and highest energy states, due to the surface atoms. However, these surface effects are negligible. The D_p obtained by the GGA with XDM model is presented for comparison or predictions with different functionals (see Section II).

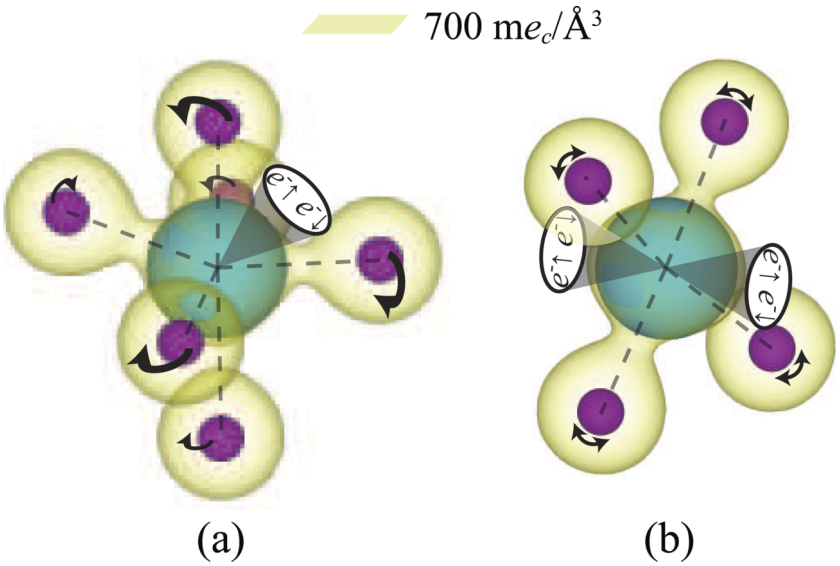

FIG. 2. The calculated transient molecular structures of (a) XeF_6 and (b) XeF_4 with their charge density distributions. The lone electron pair of XeF_6 transits, i.e., the six Xe-F bonds show continuous motion around Xe. However, the four Xe-F bonds of XeF_4 do not show continuous motion due to the intact octahedron structure, but will oscillate at their stable position.

of Xe are excited to the 5*d* orbital and hybridized as sp^3d^3, and form the molecular orbital with *p* orbitals of six F atoms. Owing to the repulsive lone pair, Xe-F bonds are displaced and gaseous XeF_6 has a distorted octahedron[17,18] with continuously changing bond lengths and angles. Contrary to XeF_6, XeF_4 has six sp^3d^2 hybridized orbitals, thus an intact octahedron structure and is more stable (Fig. 2(b)).

II. CALCULATION METHODS

The *ab initio* calculations are implemented by the Vienna *ab initio* Simulation Package (VASP)[19] and the Quantum Espresso (QE) packages.[20] VASP is used for the structure relaxation and electron density of states calculations, the *ab initio* molecular dynamics (AIMD) simulations, the reaction pathways and energies, and the F/h-BN vibration modes. The Perdew-Zunger[21] local density approximation (LDA) for the exchange-correlation functional is used[8,9,11–13,22] along with the projector augmented wave (PAW) method[23,24] with 500 eV and 400 eV cut-off energy for unit cell and supercell, respectively, due to the calculation cost. The Γ-centered grids with $11 \times 11 \times 4$ $\boldsymbol{k}$-points is used for the structure relaxation of unit cell which consists of two formula units, and the relaxed structure is used to calculate the electron density of states with expanded $44 \times 44 \times 16$ $\boldsymbol{k}$-points for accuracy. The relaxation calculations for bulk and surface supercell structures are implemented with the Γ-centered grids with 2×2×2 and $2\times2\times1\boldsymbol{k}$-points, respectively, and only the Γ point is used for the AIMD calculations.[1,25] The Γ-centered grids is strongly recommended for hexagonal structures due to a significantly faster convergence as well as a protection against hexagonal symmetry breakage.[26] The h-BN thin film rectangular supecell for the AIMD calculations consists of 4 layers with 60 atoms per each plane, and the lowest layer is fixed. The XeF_6 molecule departs at 12 Å from the surface, and the supercell size $12.5 \times 12.9 \times 33.6$ Å^3 is large enough for molecule not to be affected by periodic boundary conditions. The AIMD is implemented with canonical ensemble (*NVT*) under the Nosé-Hoover thermostat at prescribed temperature. The equilibrium calculations with fixed Xe atom were implemented for 4 ps prior to the translation/reaction calculations. A 1 fs time step is used since the nonadiabatic effects of the dissociative chemisorption are negligible.[27,28] The QE is used to calculate the D_p and three-phonon interaction rates. The Troullier-Martins method[29] (cut-off energy = 70 Ry[30]) is employed with the Perdew-Wang[31] LDA exchange-correlation functional, and automatic

$8 \times 8 \times 3\boldsymbol{k}$-points and $6 \times 6 \times 3\boldsymbol{k_p}$-points are used for D_p calculations. Detail calculation method for the three-phonon interaction rates are summarized below.

The crystal Hamiltonian is[7,32,33]

$$H = \sum_i \frac{\boldsymbol{p}_i^2}{2M_i} + \langle\varphi\rangle = \sum_i \frac{\boldsymbol{p}_i^2}{2M_i} + \langle\varphi\rangle_\circ + \frac{1}{2!}\sum_{ijxy}\Gamma_{ij}^{xy} d_i^x d_j^y + \frac{1}{3!}\sum_{ijkxyz}\Psi_{ijk}^{xyz} d_i^x d_j^y d_k^z + \cdots, \quad (1)$$

where i (or j,k) is the atomic index, x (or y,z) is the Cartesian coordinate, M_i and $\boldsymbol{p}_i$ are the mass and momentum of atom i, $\langle\varphi\rangle_\circ$ is the equilibrium potential energy, d_i^x is the displacement of atom i in x direction, and Γ_{ij}^{xy} and Ψ_{ijk}^{xyz} are the second- and third-order force constants. The second-order force constants determine the frequencies and eigenvectors of phonons, whereas the third-order force constants are related to the phonon lifetime and higher-order terms can be neglected.[34] From the Fermi golden rule, the downconversion rate by three-phonon interaction (from phonon $\boldsymbol{k}_p\alpha$ to phonons $\boldsymbol{k}_p'\alpha'$ and $\boldsymbol{k}_p''\alpha''$) is[33,35,36]

$$\begin{aligned}\dot{\gamma}_{p-p,\boldsymbol{k}_p\alpha} = \frac{1}{N_{\boldsymbol{k}_p'}}\sum_{\alpha'\alpha''\boldsymbol{k}_p'\boldsymbol{k}_p''}\frac{\pi\hbar}{16}\left|\Psi_{\alpha\alpha'\alpha''}^{\boldsymbol{k}_p\boldsymbol{k}_p'\boldsymbol{k}_p''}\right|^2\Delta_{\boldsymbol{k}_p\boldsymbol{k}_p'\boldsymbol{k}_p''}\delta(\omega_{\boldsymbol{k}_p\alpha}-\omega_{\boldsymbol{k}_p'\alpha'}-\omega_{\boldsymbol{k}_p''\alpha''}) \\ \times(f_{p,\boldsymbol{k}_p'\alpha'}+f_{p,\boldsymbol{k}_p''\alpha''}+1),\end{aligned} \quad (2)$$

where $N_{\boldsymbol{k}_p'}$ is the number of $\boldsymbol{k}_p'$ points, $\Delta_{\boldsymbol{k}_p\boldsymbol{k}_p'\boldsymbol{k}_p''}$ represents the momentum conservation, and $\Psi_{\alpha\alpha'\alpha''}^{\boldsymbol{k}_p\boldsymbol{k}_p'\boldsymbol{k}_p''}$ is the three-phonon interaction matrix element given by

$$\Psi_{\alpha\alpha'\alpha''}^{\boldsymbol{k}_p\boldsymbol{k}_p'\boldsymbol{k}_p''} = \sum_{ijk}\sum_{xyz}\left(\frac{\varepsilon_{xi}^{\boldsymbol{k}_p\alpha}\varepsilon_{yj}^{\boldsymbol{k}_p'\alpha'}\varepsilon_{zk}^{\boldsymbol{k}_p''\alpha''}}{M_iM_jM_k\omega_{\boldsymbol{k}_p\alpha}\omega_{\boldsymbol{k}_p'\alpha'}\omega_{\boldsymbol{k}_p''\alpha''}}\right)\Psi_{ijk}^{xyz}\exp\left[\imath(\boldsymbol{k}_p\cdot\boldsymbol{r}_i+\boldsymbol{k}_p'\cdot\boldsymbol{r}_j+\boldsymbol{k}_p''\cdot\boldsymbol{r}_k)\right], \quad (3)$$

where $\varepsilon_{xi}^{\boldsymbol{k}_p\alpha}$ is the component x of the eigenvector for mode $\boldsymbol{k}_p\alpha$ and atom i, and $\boldsymbol{r}_i$ is the lattice vector associated with atom i. Considering lifetimes of phonon modes only at Γ point, the equations can be treated more readily by $\boldsymbol{k}_p' = -\boldsymbol{k}_p''$ from the momentum conservation.[36] Also, a single-layer h-BN sheet is considered to obtain force constants with efficiency, considering that the in-plane interaction is much stronger than cross-plane interaction which results in much higher interaction rates and thus phonons are prone to downconvert through in-plane interactions. The density functional perturbation theory (DFPT)[37] with the 2n + 1 formula[38] was used for evaluating the third-order force constants, and the QE package was adopted with $11 \times 11 \times 1$ $\boldsymbol{k}$- and $\boldsymbol{k}_p$-points. It was verified that the self-consistent energy and the phonon density of states do not change with respect to $\boldsymbol{k}$- and $\boldsymbol{k}_p$-points. The high thresholds are used to obtain the accurate third-order force constants, 10^{-12} Ry for phonon self-consistent calculations and 10^{-8} Ry for iterative diagonalization. The obtained third-order force constants are interpolated onto $100 \times 100 \times 1\boldsymbol{k}_p$-points[36] and the Lagrangian δ-function is used with 0.1 THz smearing in the equation.

The generalized gradient approximation (GGA) is believed to be more accurate than the LDA in many cases, however it is shown that the GGA can fail to describe the weak intermolecular forces and leads to no binding between the planes.[11] A similar behavior is found for graphite which has the same structure as the h-BN.[11] Also, the GGA predicts the h-BN lattice dynamical properties rather poorly.[9] Our examinations hold the previous claims that the across-plane lattice constant relaxed by the GGA-PBE[39] with the PAW method is c = 8.13 Å, significantly larger than the experiment (6.69 Å). However, the dispersion correction functionals can enhance the performance of the GGA. Using the DFT-D3 model[40,41] with the VASP, the relaxed lattice constant is c = 6.58 Å, as accurate as the result presented with the LDA. The predicted h-BN band structure and gap are almost the same as those predicted by the LDA (not reported here). Using the XDM model[42,43] with the QE, we found that the phonon D_p is also the same as that predicted by LDA, as presented in Fig. 1. Thus, the electron and phonon properties obtained by the GGA with dispersion correction functionals are similar to those predicted by the LDA. In addition, most of reports[8,9,11–13,22] have used the LDA

functional for the study of the h-BN. Therefore, it is believed that the LDA is as accurate as the GGA with dispersion correction functional models, for our system.

III. RESULTS

A. Reaction pathway

The climbing image nudged elastic band (CI-NEB) method,[44] which searches to find the saddle point, as well as the minimum energy path for reactions by estimating the tangent to the path at each image, was adopted for the reaction pathway[45,46] shown in Fig. 3, where the end states I to V were obtained by relaxation and I is set as the reference. The calculated molecular adsorption (physisorption) energy is 191 meV between states I and II and is downconverted to lower energy phonons with transfer in the in-plane direction rather than cross-plane, due to the strong coupling of in-plane B and N. Between IV and V the desorption energy of XeF_4 is larger than the physisorption of XeF_6 because of the XeF_4 interaction with two F/h-BN bonds, shown in the snapshot IV with larger charge density difference compared to snapshot II (compared to 156 meV for XeF_4 on the clean h-BN surface from our *ab initio* calculations).

The activation energy for dissociating F atom, II to transition state (TS), is 372 meV with steep activation ascent. The gradual climb from II to the position beneath ② is readily achieved by absorption of 41 meV phonons which have the highest population shown in Fig. 5(a1). The dissociation process requires overcoming the steep ascent to TS by absorbing the remaining energy of 331 meV which can be by absorbing two phonons (e.g., two 165.5 meV) from the high-energy optical phonons of h-BN between 150 to 200 meV. The dissociation would have a very low probability of occurrence when the surface cannot supply the proper high-energy phonons, noting the significantly lower rates involving three or more phonons.

Between TS and III the energy emitted is 121 meV, low considering the formation of F/h-BN covalent bond, but there yet remain five F atoms around Xe, so Xe atom cannot make a stable structure and this instability offsets the chemisorption energy.

During the XeF_4 formation, the 2nd F is dissociated and the 2nd F/h-BN bond is formed. With no TS between III/IV, no extra energy for the dissociation of 2nd F atom is required, since this F disengages spontaneously from the unstable molecule, and energy decreases continuously and significantly as XeF_4 and 2nd F/h-BN bond are formed. The pathway between III/IV is not a linear

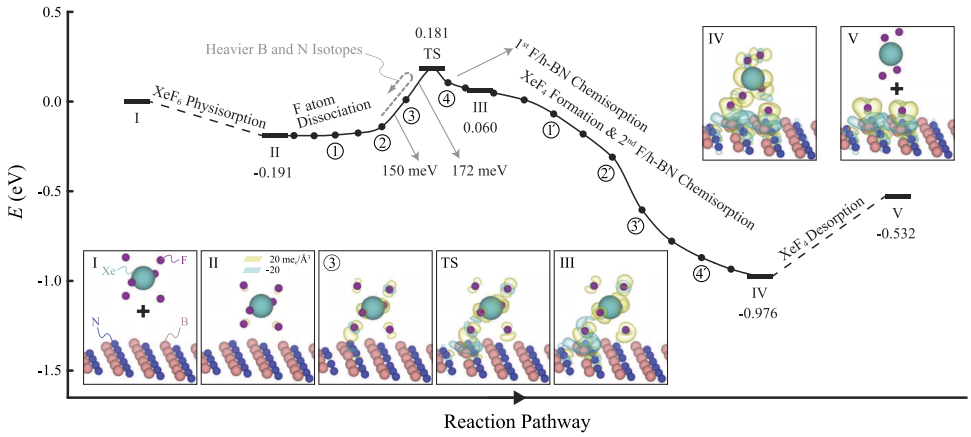

FIG. 3. Reaction pathway for XeF_6 physisorption, F/h-BN chemisorption, and XeF_4 formation/desorption, with AIMD snapshots showing the charge density difference plots. The CI-NEB method was implemented between II/III and III/IV with 9 images. The transition state (TS) due to F dissociation is seen only in the 1st chemisorption. The dotted gray arrow returning to state II is the path for the case of the heavier B and N isotopes. The plus sign in the snapshots for I and V denotes that the surface and the molecule are completely separated. The circular numbers correspond to the number of snapshots and are also used in Movie I.[54]

line but an inverted S-curve showing gradual interaction between F and B followed by increased interaction between (2′) and (3′), and complete F/h-BN bond at (4′), see Movie I.[54]

B. AIMD simulations and spectral analysis

The AIMD (molecule in thermal equilibrium with the surface) results show the dissociative chemisorption reaction occurs over 500 K, while physisorption does not occur over 800 K, i.e., the dissociative sticking probability decreases exponentially as the substrate temperature is lowered.[47] We report results for 600 K and 200 m/s molecular speed (most probable speed in the Maxwell-Boltzmann distribution,[7] equivalent to 51 meV), conditions for dissociation of F and formation of F/h-BN (Movie II[54]). To demonstrate the role of phonons, progressively heavier B and N isotopes are used for the control of chemisorbed dissociation by a controlled study of the substrate phonons. With 1.2 times larger masses the reaction continues to occur (Movie III[54]), while with 1.5 times larger masses the dissociation does not occur, under otherwise the same conditions (Movie IV[54]). Here we present comparison results for normal B and N atoms and 1.5 times heavier isotopes.

Figure 4 is history of the z-direction displacement-square of targeted B, $\Delta^2_{B,z}$, and as XeF_6 approaches the surface $\Delta^2_{B,z}$ becomes larger and the physisorption occurs, for both cases. The physisorption interaction of XeF_6 with surface is weak, so the charge density difference is small compared to the dissociative chemisorption. After 2.8 ps, in Fig. 4(a), with the normal atoms the dissociative chemisorption occurs rapidly within 32 fs and the electron density difference shows the F/h-BN bond formation. The results are in agreement with reported result[48] that the time required for exchange of energy with phonons is about 35 fs. The $\Delta^2_{B,z}$ history manifests the reaction, suggesting that vibrational mode of the targeted B atom is changed (increased frequency). The XeF_4 is formed and begins desorbing after 400 fs. Contrary to the normal B and N, the heavier isotopes cannot trigger reaction (dissociation) and XeF_6 remains adsorbed on the surface, thus no frequency variation is identified in Fig. 4(b).

To analyze the transient energy transfer, fast Fourier transform (FFT) is applied to the displacement of targeted B, over 2800 steps (2.8 ps) for each event, in Fig. 5. The x and z-direction results show similar spectral behavior as the phonon population ($D_p f_p^o$), where f_p^o is equilibrium phonon

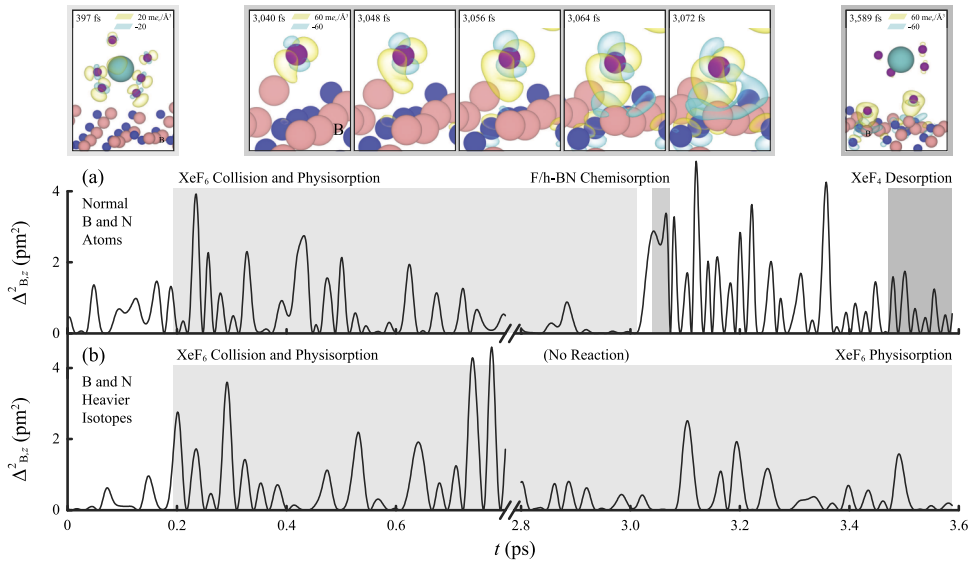

FIG. 4. The history of z-direction displacement-square of targeted B (a) for normal B and N with snapshots showing the charge density difference plots, and (b) for B and N heavier isotopes. The initial time is when XeF_6 is near the surface. The regimes durations are shaded. XeF_6 is chemisorbed with the normal atoms after physisorption, but heavier isotopes do not allow for dissociative chemisorption (only physisorption). The results are for 600 K.

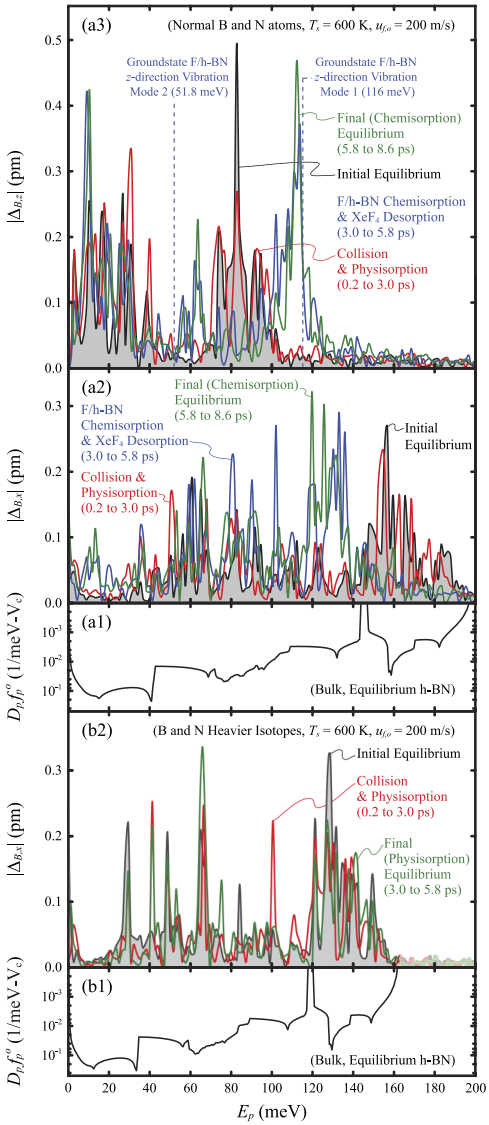

FIG. 5. Transient spectral analysis of displacement of targeted B (a) for normal B and N, and (b) for heavier isotopes. (1) Phonon population, (2) FFT for the x direction, and (3) FFT for the z direction, with F/h-BN vibration modes also shown. The F/h-BN chemisorption changes the distribution of phonons dramatically, but phonon energy bands of heavier isotopes remain almost the same. Phonon energies over 162 meV do not exist in the heavier B and N lattice. Note that the lightly shaded region in (b2) is not physical (due to the FFT scatter/noise).

occupancy. The excited high-energy optical phonons are in the x direction (in-plane), while most of excited phonons in the z direction (cross-plane) are low energy. The F atom dissociation in Movie II[54] accompanies absorption of these high-energy phonons in Fig. 5(a2).

Comparing FFTs for different elapsed times, phonon energy peaks change, e.g., physisorption and exothermic reactions absorb and emit phonons. Also, the phonon up/downconversions change the phonon nonequilibrium occupancy. For example, the difference between the black and red curves in Fig. 5 is not only associated with the energy absorption from the collision (kinetic energy, 51 meV) and physisorption (191 meV) of XeF_6 on the h-BN surface, but also the consequent phonon up/downconversion within the elapsed time leading to equilibrium occupancy. To assess the up/downconversion affecting the occupancy between events (2.8 ps), the three-phonon interaction rates are calculated with the *ab initio* method (Section II). The rates are 0.78, 0.88, and 0.50 ps at 600 K for the downconversions of optical phonons of 102, 170, and 190 meV, respectively, at the

Γ point. Therefore, some three-phonon interactions can occur between the events and the phonon occupancy is affected by these interactions.

After the chemisorption, in Fig. 5(a2), the vibrations between 150 to 180 meV are significantly damped and those between 120 to 140 meV and the peaks at 100, 90, and 80 meV appear. The vibrations in 120 to 140 meV result from the phonon redshift of those in 150 to 180 meV, due to the F/h-BN bond formation. This is because the F/h-BN bond pulls the B atom and hinders the in-plane vibration, thus has a bond softening effect. Therefore, the vibrations between 120 to 140 meV persist in the final equilibrium, as shown in Fig. 5(a2). Contrary to these, the three peaks from the absorption of the net energy by the F/h-BN chemisorption and the XeF_4 formation/desorption, are damped later by the relaxations.

In Fig. 5(a3), the vibrations between 70 to 90 meV are considerably decreased and those between 100 to 120 and at 60 meV appear after the chemisorption. The result suggests that the main vibration mode of B in the z direction is changed to these new modes by the F adatom. The two F/h-BN z-direction vibration modes (fundamental) are evaluated by fixing all atoms except the B and F vibrating around their equilibrium position. Interestingly, these restricted condition modes coincide with the dynamic peaks. Also, the final equilibrium shows that the modes remain, confirming that these peaks are due to the F/h-BN. The fundamental vibration modes from vibrational spectroscopy with neutrons and their simulations for molecules/atoms adsorbed on catalysts, show spectra similar to these peaks.[49]

The phonon cutoff energy for the heavier isotopes is reduced by 20% as shown in Fig. 5(b1) (to 162 meV, $\omega \propto m^{-1/2}$),[7] and the dissociation did not occur as shown in Movie IV.[54] The final equilibrium in Fig. 5(b2) shows that vibrations do not change considerably (also there is no phonon over 155 meV, the same as the equilibrium phonon population). Phonon energy over 165.5 meV is required for the dissociation of XeF_6 accompanied with two-phonon absorption. So, it is expected that the case of the heavier B and N isotopes cannot overcome the activation energy for the dissociation by a two-phonon absorption and the XeF_6 molecule stays in state II, as shown in Fig. 3 by the dotted gray arrow returning to state II. The probability of mutiphonon absorption is a product probability, so, as the number of participating phonons increases this probability substantially decreases. So, the possibility of F/h-BN chemisorption for the case of heavy isotopes is substantially lower than that for the normal atoms. 1.2 times larger atomic masses (Movie III[54]) supports that a 9% reduction in the cutoff energy (to 182 meV) does not inhibit the reaction. This shows that when the phonon cutoff energy is below the required dissociation phonon energy, the reaction does not occur. Therefore, this catalytic-chemisorption reaction, dominated by phonon energy transfer, is controlled by the substrate phonons, i.e., controllable phonocatalysis.

In general, the condition where the heavier surface isotopes can be used to achieve the control is rooted in the required phonon energy as determined by the reaction pathway (the activation energy) and the substrate phonon cutoff energy (available high-energy phonons). The control of the dissociative chemisorption was demonstrated using heavy isotopes (lower phonon cutoff energy below the required minimum phonon energy for the dissociation by two-phonon absorption), which shows dissociation is favorable when the required phonon energy is near/below the cutoff energy. So we suggest that the condition for use of the heavier surface isotopes is when the required minimum phonon energy is in the high-energy optical phonon regime (near cutoff). Per phonon D_p, the most populated optical-phonon peak is absorbed, so it is preferred for the peak to be located above the required phonon energy. This leads to dissociation with the phonon absorption probability being higher for the normal atoms. So the difference in the reaction rate between the normal atoms and the isotopes becomes more pronounced and the control using isotopes is very effective.

IV. CONCLUSIONS

The self-consistent, accurate *ab initio* simulations of phonocatalysis dynamics offer insight into the controlled chemisorbed reactions with the critical role of the optical phonons. We showed that the heterogeneous reaction (chemisorbed dissociation) on large bandgap semiconductor surface can be controlled by its phonons. In our example of the XeF_6 dissociation in h-BN, two high-energy phonons are absorbed to overcome the activation energy. In the case of heavier B and N isotopes,

however, the contribution of three or more low-energy phonons are necessitated for the pathway ascent, due to the lack of high-energy optical phonons required for the reaction by two-phonon absorption. Since the reaction probability decreases with the required number of phonons (a product probability for multiphonon participation), the reduction in phonon cutoff energy and resort to the multiphonon absorption option is critical in this reaction dynamics and will prohibit the reaction. For h-BN, the three-phonon interaction times for the high-energy optical phonons at the Γ point are under 1 ps (at 600 K) and tracking of the instantaneous displacement of surface atoms shows that the reaction takes place in less than 0.1 ps.

In addition to the isotope control shown here, phonons can be controlled by heterogeneous layered structures with the surface layer providing the surface-reaction-mediation effect (force field) and the subsurface layer mediating with the required, control phonons (with strong interlayer coupling).

These simulation studies can be further advanced by taking advantage of the femto-/attosecond laser techniques.[50–53] From the experiments of femtosecond laser-induced oxidation of CO on Ru(100), the CO oxidation driven by an electronic excitation (fast response) and the CO desorption coupled with phonons (slow response) were distinguished.[50] Also, the two-step mechanism of the CO desorption on Ru(0001) has been demonstrated.[51,52] The state-of-the-art attosecond technology has delved into the dissociative dynamics of N_2^+.[53] So, phonocatalysis can be used in short-lived sorption and reaction processes and observed with time-resolved techniques.

ACKNOWLEDGMENTS

We are thankful to Professor G. Henkelman for insightful suggestions on the reaction pathway calculations. This work was supported by the NSF program on Thermal Transport and Processes (Award No. CBET1332807) and employed computing resources of the DOE National Energy Research Scientific Computing Center (Office of Science, Contract No. DE-AC02-05CH11231).

[1] A. Groβ, Phys. Rev. Lett. **103**, 246101 (2009).
[2] B. N. J. Persson and R. Ryberg, Phys. Rev. B **40**, 10273 (1989).
[3] T. A. Westrich, K. A. Dahlberg, M. Kaviany, and J. W. Schwank, J. Phys. Chem. C **115**, 16537 (2011).
[4] J. R. Manson, Handbook of Surface Science **3**, 53 (2008).
[5] C. J. Hagedorn, M. J. Weiss, and W. H. Weinberg, Phys. Rev. B **60**, 14016 (1999).
[6] C. T. Rettner, D. J. Auerbach, J. C. Tully, and A. W. Kleyn, J. Phys. Chem **100**, 13021 (1996).
[7] M. Kaviany, *Heat Transfer Physics*, 2nd ed. (Cambridge University Press, New York, 2014).
[8] L. Liu, Y. P. Feng, and Z.X. Shen, Phys. Rev. B **68**, 104102 (2003).
[9] B. Altintas, C. Parlak, C. Bozkurt, and R. Eryiğit, Eur. Phys. J. B **79**, 301 (2011).
[10] R. Arenal and A. Lopez-Bezanilla, WIREs Comput. Mol. Sci. **5**, 299 (2015).
[11] G. Kern, G. Kresse, and J. Hafner, Phys. Rev. B **59**, 8551 (1999).
[12] L. Wirtz, A. Rubio, R. A. delaConcha, and A. Loiseau, Phys. Rev. B **68**, 045425 (2003).
[13] J. Serrano, A. Bosak, R. Arenal, M. Krisch, K. Watanabe, T. Taniguchi, H. Kanda, A. Rubio, and L. Wirtz, Phys. Rev. Lett. **98**, 095503 (2007).
[14] H. Sevinçli, W. Li, N. Mingo, G. Cuniberti, and S. Roche, Phys. Rev. B **84**, 205444 (2011).
[15] X. L. Ruan and M. Kaviany, Phys. Rev. B **73**, 155422 (2006).
[16] H. Bao, X. L. Ruan, and M. Kaviany, Phys. Rev. B **78**, 125417 (2008).
[17] L. S. Bartell and R. M. Gavin, Jr., J. Chem. Phys. **48**, 2466 (1968).
[18] R. K. Sharma, *Chemistry of Hydrides and Carbides* (Discovery Publishing House, New Delhi, 2007).
[19] G. Kresse and J. Furthmüller, Phys. Rev. B **54**, 11169 (1996).
[20] P. Giannozzi *et al.*, J. Phys. Condens. Mat. **21**, 395502 (2009).
[21] J. Perdew and A. Zunger, Phys. Rev. B **23**, 5048 (1981).
[22] H. P. Koch, R. Laskowski, P. Blaha, and K. Schwarz, Phys. Rev. B **84**, 245410 (2011).
[23] P. E. Blöchl, Phys. Rev. B **50**, 17953 (1994).
[24] G. Kresse and D. Joubert, Phys. Rev. B **59**, 1758 (1999).
[25] H. Kim, M. H. Kim, and M. Kaviany, J. Appl. Phys **115**, 123510 (2014).
[26] G. Kresse, M. Marsman, and J. Furthmüller, VASP the GUIDE (http://cms.mpi.univie.ac .at/vasp/vasp/vasp.html, 2015).
[27] P. Nieto, E. Pijper, D. Barredo, G. Laurent, R. A. Olsen, E-J. Baerends, G-J. Kroes, and D. Farias, Science **312**, 86 (2006).
[28] J. I. Juaristi, M. Alducin, R. Díez Muiño, H. F. Busnengo, and A. Salin, Phys. Rev. Lett. **100**, 116102 (2008).
[29] N. Troullier and J. L. Martins, Phys. Rev. B **43**, 1993 (1991).
[30] J. S. Arellano, J. Phys.: Conference Series **582**, 012060 (2015).
[31] J. P. Perdew and Y. Wang, Phys. Rev. B **45**, 13244 (1992).
[32] G. P. Srivastava, *The Physics of Phonons* (Adam hilger, Bristol, 1990).
[33] O. Hellman and I. A. Abrikosov, Phys. Rev. B **88**, 144301 (2013).

[34] D. Ecsedy and P. Klemens, Phys. Rev. B **15**, 5957 (1977).
[35] S. Shin and M. Kaviany, Phys. Rev. B **91**, 165310 (2015).
[36] C. Melnick and M. Kaviany, Phys. Rev. B **93**, 125203 (2016).
[37] S. Baroni, S. de Gironcoli, A. D. Corso, and P. Giannozzi, Rev. Mod. Phys. **73**, 515 (2001).
[38] X. Gonze and J. -P. Vigneron, Phys. Rev. B **39**, 13120 (1989).
[39] J. P. Perdew, K. Burke, and M. Ernzerhof, Phys. Rev. Lett. **77**, 3865 (1996).
[40] S. Grimme, J. Antony, S. Ehrlich, and S. Krieg, J. Chem. Phys. **132**, 154104 (2010).
[41] S. Grimme, S. Ehrlich, and L. Goerigk, J. Comp. Chem. **32**, 1456 (2011).
[42] A. D. Becke and E. R. Johnson, J. Chem. Phys. **127**, 154108 (2007).
[43] A. Otero de la Roza and E. R. Johnson, J. Chem. Phys. **136**, 174109 (2012).
[44] G. Henkelman, B. P. Uberuaga, and H. Jonsson, J. Chem. Phys. **113**, 9901 (2000).
[45] M. Garcia-Melchor and N. Lopez, J. Phys. Chem. C **118**, 10921 (2014).
[46] Y-G. Wang, D. Mei, V-A. Glezakou, J. Li, and R. Rousseau, Nat. Commun. **6**, 6511 (2015).
[47] R. D. Muino and H. F. Busnengo, *Dynamics of Gas-Surface Interactions* (Springer-Verlag, Berlin, 2013).
[48] T. Sahoo, S. Sardar, and S. Adhikari, Phys. Scr. **84**, 028105 (2011).
[49] H. H. Brongersma and R. A. van Santen, *Fundamental Aspects of Heterogeneous Catalysis Studied by Particle Beams* (Plenum Press, New York, 1991).
[50] C. Hess, S. Funk, M. Bonn, D. N. Denzler, M. Wolf, and G. Ertl, Appl. Phys. A **71**, 477 (2000).
[51] M. Beye *et al.*, Phys. Rev. Lett. **110**, 186101 (2013).
[52] M. Dell'Angela *et al.*, Science **339**, 1302 (2013).
[53] A. Trabattoni *et al.*, Phys. Rev. X **5**, 041053 (2015).
[54] See supplementary material at http://dx.doi.org/10.1063/1.4955054 for Movie I (snapshot movie obtained from reaction pathway calculations) and Movie II – IV (AIMD results for dissociative chemisorption with different atomic masses of h-BN thin film).